Nano Energy 71 (2020) 104612

Contents lists available at ScienceDirect

Nano Energy

journal homepage: http://www.elsevier.com/locate/nanoen

Full paper

# Shape matters: Enhanced osmotic energy harvesting in bullet-shaped nanochannels

Gregorio Laucirica [a], Alberto G. Albesa [a], María Eugenia Toimil-Molares [b], Christina Trautmann [b,c], Waldemar A. Marmisollé [a,**], Omar Azzaroni [a,*]

[a] Instituto de Investigaciones Fisicoquímicas Teóricas y Aplicadas (INIFTA)[1] – Departamento de Química – Facultad de Ciencias Exactas – Universidad Nacional de La Plata (UNLP) – CONICET, Diagonal 113 and 64, La Plata, 1900, Argentina
[b] GSI Helmholtzzentrum für Schwerionenforschung, 64291, Darmstadt, Germany
[c] Technische Universität Darmstadt, Materialwissenschaft, 64287, Darmstadt, Germany

ARTICLE INFO

*Keywords:*
Concentration polarization
Nanofluidics
Ion transport
Osmotic power generation
Blue energy

ABSTRACT

Nanofluidic reverse electrodialysis systems based on track-etched nanochannels are promising devices for new eco-friendly ways of sustainable energy generation. In recent years, several works have been focused on the influence of parameters such as pH, ionic strength, and chemical nature of the electrolyte on the device performance. However, despite the relevance of the geometry on the channel properties, the influence of the nanochannel shape on the performance of energy conversion remains almost unexplored. In this work, we present an experimental study – complemented with Poisson–Nernst–Planck simulations – that describes how the shape of the nanochannels strongly affects the energy conversion performance of single bullet-shaped nanochannels created on PET foils by the ion-track-etching method. To test optimal parameters for energy conversion and selectivity, the performance was investigated by varying the channel effective diameter as well as the pH and the electrolyte gradient. With a maximum output power of 80 pW, this system reveals the best value reported for a bare single track-etched nanochannel. Therefore, this work experimentally demonstrates that it is possible to obtain high power output by means of a careful choice of channel geometry and etching conditions, in addition to other experimental parameters such as pH and electrolyte gradient. We believe that these results offer a promising framework to explore new design concepts in nanofluidic osmotic power generators.

## 1. Introduction

The increase of energy demand, as well as the concern for the high environmental impact of the use of fossil fuels, encouraged the study and the development of new ways for eco-friendly energy generation. The search for new alternatives for energy harvesting systems with low environmental impact is a great ongoing effort [1–3]. The development of a system that generates energy from mixing water with different salinity content (e.g. seawater and river water) has attracted considerable attention because of its great attributes such as having a low environmental impact, low cost and accessibility [4,5]. As an example, reverse electrodialysis (RED) is a method that allows pursuing these goals [6,7]. RED consists in the transformation of Gibbs free energy of mixing, obtained when mixing freshwater and saltwater, into electrical energy [8]. This conversion is obtained from the generation of an electrochemical potential by the action of an ion-selective membrane disposed between two reservoirs with different electrolyte concentrations (activities) [9–11]. The key factor of any RED device is the membrane performance in terms of resistance and ion-selectivity; that is why new strategies and materials for enhancing the membrane selectivity become a relevant issue in clean energy production [12].

Nowadays, great improvement is being achieved in the development of renewable energy sources by the use of nanotechnology [13–15]. Bottom-up strategies with size and shape-controlled building blocks can enhance the performance of solar-cells, RED systems, batteries, among others [12,16–19]. Regarding reverse electrodialysis, the great advances in nanofabrication have outlined the design of solid-state nanochannels (SSN) as an easy and effective way for the generation of salinity gradient

* Corresponding author.
** Corresponding author.
*E-mail addresses:* wmarmi@inifta.unlp.edu.ar (W.A. Marmisollé), azzaroni@inifta.unlp.edu.ar (O. Azzaroni).
[1] web: https://softmatter.quimica.unlp.edu.ar/; twitter: @softmatterlab

https://doi.org/10.1016/j.nanoen.2020.104612
Received 3 January 2020; Received in revised form 27 January 2020; Accepted 11 February 2020
Available online 13 February 2020

energy [20–23]. In recent years, several salinity-gradient power generation systems based on SSN from different materials, such as alumina, silicon-based, copolymer blocks and polymer membranes such as polyimide (PI), polycarbonate and poly(ethylene terephthalate) (PET), have been introduced [24–33].

Nanochannels created by the ion-track-etching method have gained special attention since they have demonstrated a great potential for harvesting energy via RED [20,24,29–31,34]. Pioneering works by Siwy et al. and Cervera et al. showed that the exposition of a track-etched nanochannel to a concentration gradient generates a junction potential and a zero-volt current [11,35]. This principle was taken by Guo et al. with the aim of designing an ion-selective membrane for reverse electrodialysis based on track-etched nanochannels. These researchers studied the energy-conversion performance of PI conical channels varying both the pH and the size of the channel and demonstrated a power up to 26 pW for the optimized nanochannels dimensions. Assuming a linear scaling up to high pore densities, their result would yield an improvement of three orders of magnitude compared to commercial RED membranes [34]. However, recent experiments show that scaling up to high pore densities does not follow a linear relation and the resulting energy production is lower than that expected [36,37]. However, with the aim of shedding light on which are the factors that can substantially improve the performance, the study in single-pore systems is still an appropriate platform.

Studies on single-pore systems are extremely helpful in revealing critical channel parameters that may affect the performance of nanofluidic reverse electrodialysis (nRED) devices [11,38–42]. For example, Cao et al. carried out a systematic investigation of the electrolyte ions and the charge selectivity using conical nanochannels. They found that the performance is directly related to the ion diffusion number. For cation-selective nanochannels, KF as electrolyte showed the best performance, whereas for anion-selective nanochannels the best results were obtained with LiCl [43]. Tseng et al. studied the influence of size and gradient concentration in the output power generated by nRED. They concluded that a reduction of both the radius and the length of the pore, together with an increase of the gradient concentration, maximizes the power output [41]. However, a significant decrease of the channel length below 400 nm is detrimental [44,45]. Several theoretical works based on Poisson-Nernst-Planck (PNP) simulations investigated the impact of the shape of the nanochannel [38,40]. In this regard, the design of nanochannel with asymmetric geometries leads to an increment in the power due to the decrease in the channel resistance [23,46]. Moreover, Ramírez et al. simulated conical, trumpet- and the bullet-shaped nanochannels and found that the nanochannel shape is of crucial importance as it determines both the transmembrane current and the ion selectivity of the device [47]. For channels with the same diameter, it was calculated that bullet-shaped nanochannels provide a substantial improvement in power output. However, to our knowledge, experimental studies on the power generation performance of bullet-shaped nanochannels have not been reported so far.

Here, we present the results of a comprehensive experimental study on the energy conversion performance of bullet-shaped nanochannels in PET foils created by the ion-track-etching method. Bullet-shaped nanochannels are parallel channels that significantly tapper close to the channel exit forming a very small pore mouth. This special geometry is obtained by asymmetric surfactant-assisted etching [48]. In this experimental study, we tested the power, efficiency and selectivity of the nRED system by varying the effective nanochannel diameter, as well as the pH and imposed concentration gradient of the electrolyte. With a maximum output power of 80 pW, this configuration widely exceeds the results obtained for conical channel geometries. The power generated by the present system is the highest reported for a single unmodified track-etched nanochannel. This work encourages the use of bullet-shaped nanochannels as an interesting alternative for functional systems with application in macro-scale energy conversion.

## 2. Experimental section

Nanochannel synthesis: PET foils (12 μm thick) were irradiated with a single swift heavy ion Au (2.2 GeV). Along its trajectory, each ion produces a damaged trail (track) across the foil. The track has a typical width of several nm and consists of severely damaged material [49]. Due to the high chemical reactivity, chemical etching converts tracks into open channels. The etching agent and etching condition determine the channel geometry. By the etching time, the final channel diameter can be adjusted [50,51]. As etchant, we used 6 M NaOH at a temperature of ~60 °C and the etching time was varied between 5 and 9 min. Bullet-shaped geometry of the nanochannels was obtained by adding a surfactant (Dowfax 2a1 0.05%) to the etchant on one side of the membrane (tip side) [48,52]. After stopping the etching process, the membrane was carefully rinsed in mQ water.

Conductivity measurements: the iontronic measurements were performed in a four-electrode configuration using a potentiostat (*Gamry Reference 600*) [53]. For the energy conversion experiments, three cycles of *i-V curves* with short limits of transmembrane voltage (from −50 mV to 150 mV) and a low scan rate (±5 mV $s^{-1}$) were performed. For the standard conductimetric measurements, the transmembrane potential window was varied between ±1V with a potential sweep of 100 mV $s^{-1}$.

The *i-V* curves for the analysis of energy harvesting were carried out in asymmetric conditions of electrolyte. In all cases, the half-cell in the base side was filled with KCl 1 M whereas the half-cell in the tip side was filled with solutions in the range $10^{-3}$ – 0.1 M. Unless otherwise explained, the measurements were carried out at pH~10.

Rectification factor ($f_{rec}$)**:** in order to quantify the ionic current rectification (ICR) efficiency, the $f_{rec}$ was introduced. This parameter was calculated as follow,

$$f_{rec} = \frac{I(1\ \mathrm{V})}{I(-1\ \mathrm{V})} \quad \text{if} \quad I(1\ \mathrm{V}) \geq I(-1\ \mathrm{V})$$
$$f_{rec} = \frac{I(-1\ \mathrm{V})}{I(1\ \mathrm{V})} \quad \text{if} \quad I(-1\ \mathrm{V}) \geq I(1\ \mathrm{V}) \qquad (1)$$

## 3. Results

### 3.1. Ionic current rectification

The etching procedure leads to the formation of carboxyl groups at the channel surface and is responsible for the resulting negative surface charges, which induce ionic transport selectivity at neutral and basic pH conditions [47,54,55]. On the other hand, the asymmetric etching condition produces the bullet-like shape of the nanochannel, which has a paramount relevance on the disruption of the electrical potential symmetry yielding ionic current rectification (ICR) or ionic diodes [56]. Fig. 1A shows the response of asymmetric bullet-shaped nanochannels of various diameters at moderate ionic strength and alkaline pH (KCl = 0.1 M and pH = 10). The bullet-shaped geometry was confirmed by SEM images (Fig. S1). The charged surface exposed to the electrolytic solution results in an enrichment of counter-ions in the vicinity of the surface to maintain electroneutrality. This region is commonly called electrical double layer (EDL) and its thickness, which generally is in the nanometric range, is characterized by the Debye length ($\lambda_D$). In a nanochannel with negatively charged groups, the Debye length has a comparable size as the tip diameter if the salt concentration is low enough. Ergo, the surface electric potential causes in the tip region the exclusion of anions (ions with the same sign of surface charge) and enrichment of cations (ions with the opposite sign of the surface charge) [57,58]. At this condition, the current is regulated by the surface charges (surface-governed) and is largely explained by cation transport. The asymmetric ionic transport (diode-like behavior) is characterized by the rectification factor (see Experimental section). Rectification factors for single nanochannels of different sizes are presented in Fig. 1B as a function of the ionic strength. The surface control of the ionic transport

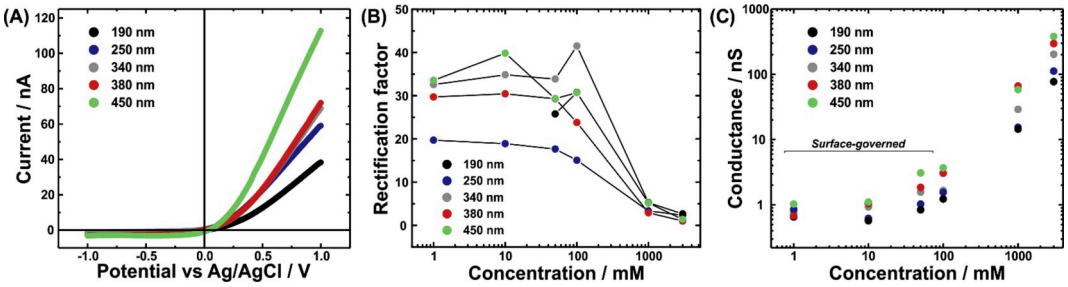


**Fig. 1.** (A) *i-V* curves for single bullet-shaped nanochannels of different diameters. The measurements were carried out in 0.1 M KCl and pH = 10. (B) Rectification factor vs. concentration of KCl at pH = 10. (C) Conductance of bullet-shaped nanochannels vs. concentration of KCl at pH = 10. In the low concentration range the conductance is dominated by surface charge, yielding a plateau. The legend indicates the effective diameters, $D_{eff}$, of the different channels.

explains the plateau in terms of conductance for low concentrations of KCl (low ionic strength) in Fig. 1B. It is important to remark that the EDL has an important influence on ionic transport, but it is not required the overlapping for triggering a surface-governed (or rectifier) behavior [59–61]. On the other hand, for salt concentration above around 1000 mM, the Debye length shrinks, and consequently, the effect of surface charges on ion transport decreases due to efficient screening. Accordingly, the iontronic output is determined for the electrolyte concentration and the geometry of the nanochannel. This condition is similar to the bulk behavior which explains the linear increment of the conductance for KCl concentrations above 100 mM in Fig. 1C [54,62]. This loss of superficial control at 1000 mM leads to the decrease of the rectification efficiency shown in Fig. 1B [58].

### 3.2. Effective size of nanochannels

To characterize the size of our bullet-shaped nanochannels, the following mathematical description is given [60].

$$D(x) = D - \left(D - d_{tip}\right)\exp(-x/h) \tag{2}$$

where x is the axis of the channel of length L, D the base diameter, $d_{tip}$ the tip diameter and $h$ a parameter that accounts for the bullet-like shape (Fig. S2).

The tip ($d_{tip}$) and base ($D$) diameters and the shape parameter $L/h$ can be deduced from the iontronic response of the nanochannels using PNP-based models [58,63]. Details of the procedure are presented in the SI file, the values of the channels tested in this study are presented in Table 1.

When considering the effect of the geometry and size on the salinity gradient-based power generation performance of the nanochannels, it is more useful to use a single effective parameter characterizing the conductance response. Thus, we computed the effective diameter, $D_{eff}$, as the diameter of a cylindrical nanochannel having the same conductance as the bullet-shaped channels at high ionic strength. These diameters were estimated for each nanochannel from the *i-V* curve measurements in a condition that ensures bulk-like behavior (and neglects nanoconfinement effects), *i. e.* high ionic strength (1 M KCl) [50], as follows [64].

$$D_{eff} = \sqrt{\frac{4L}{\pi\kappa R}} \tag{3}$$

**Table 1**
Nanochannels size characterization.

| $d_{tip}$ (nm) | D (nm) | $L/h$ | $D_{eff}$ (nm) |
|---|---|---|---|
| 10 | 1000 | 5 | 190 |
| 14 | 900 | 8 | 250 |
| 14 | 1000 | 8 | 340 |
| 30 | 1200 | 4 | 380 |
| 12 | 1900 | 9 | 450 |

where R is the resistance obtained from the *i-V* curve at low transmembrane potentials (linear region), κ is the specific conductance of 1 M KCl at 25 °C (0.11 $\Omega^{-1}cm^{-1}$) and $L$ is the channel length, which can be approximated by the thickness of the unetched foil (12 μm).

The effective diameter correlates with the bullet geometry parameters according to (see ESI for details)

$$D_{eff} \approx \left[d_{tip} D \frac{L}{h}\right]^{1/2} \tag{4}$$

Fig. 2 shows the correlation between the effective diameters determined from the experimental results of the nanochannels conductance at high salt concentration and the estimation by eq. (4) from the bullet-shaped geometry parameters determined using the PNP formalism (Table 1). It is important to note that the PNP parameters were determined from the *i-V* curves at 0.1 M KCl (diode-like, non-ohmic behavior), whereas the $D_{eff}$ values were obtained from the conductance of the nanochannels at higher ionic concentration (1 M KCl), at which confinement effects can be neglected. Finally, this correlation reinforces the utilization of $D_{eff}$ as a single parameter characterizing the size of the nanochannels.

### 3.3. Salt gradient-based energy conversion

As mentioned earlier, it has been demonstrated that the ion selectivity achieved in track-etched nanochannels provides a promising route for the development of a system that turns Gibbs free energy of mixing into electrical energy [8,34]. The experimental procedure is based on the exposition of ion-selective nanochannels to gradient concentrations.

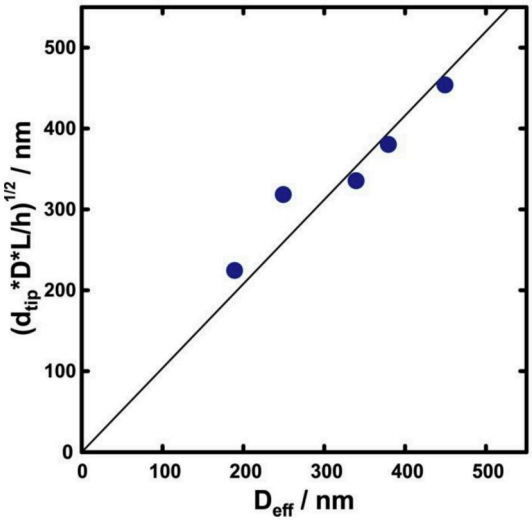


**Fig. 2.** Relation between bullet geometry parameters and effective diameters obtained by *i-V* curves.

In this condition, the Gibbs free energy forces the diffusion of ions from the solution with high activity to the solution with low activity. Since the channel surface has a defined charge, the counter-ion flux is favored in relation to the flux of co-ions, yielding net charge transport [9,10]. Concomitantly, a junction potential (diffusion potential -$E_{diff}$-) and a zero-volt current ($i_0$) are generated [11]. The iontronic output measurement in the presence of a gradient concentration yields a *i-V* curve as displaced from the origin (0; 0) in Fig. 3, right [35]. This fact is characterized by the following equation [27,38,65].

$$V = E_{diff} + IR \tag{5}$$

$E_{diff}$ can be approximated as the reversal potential ($V_{rev}$) in the absence of redox processes on the electrode surface (this fact will be discussed later). $V_{rev}$ is defined as the potential in which the current is zero (Fig. 3, right).

From $E_{diff}$, (or $V_{rev}$), it is possible to deduce the system selectivity with the cation and anion transference number [9,10],

$$t_+ = \frac{1}{2}\left[1 + \frac{F}{RT}\frac{E_{diff}}{\ln(a_H/a_L)}\right] \tag{6}$$

$$t_- = 1 - t_+ \tag{7}$$

where $a_H$ and $a_L$, denote the respective activities in the reservoir filled with solutions of high (H) and low (L) activities (see Fig. 3, left). *F*, *T,* and *R* are the Faraday constant, the temperature (room temperature) and the gas constant, respectively. It is important to clarify that transference numbers were calculated using activity values instead of concentrations employing reported activity coefficients at each condition [66].

Experimentally the measurements consisted of recording *i-V* curves in the presence of an electrolyte gradient for bullet-shaped nanochannels of different diameters due to different etching times. The half-cell compartment on the base side of the channel was filled with a 1 M KCl ($C_H$) solution, whereas the KCl concentration of the reservoir on the tip side was varied between 1 and 100 mM ($C_L$). The disposition of the most concentrated KCl in the base side produces an improvement in the performance of the energy conversion system [11]. Moreover, KCl salt enhances the energy conversion performance of cation-selective systems compared to NaCl and LiCl [43]. Our experimental set-up involved a four-electrode array formed by two Pt electrodes –working and counter electrode- and two Ag/AgCl electrodes –reference and working sense- connected to a potentiostat. As the Ag/AgCl electrodes were immersed in saturated KCl bridges, it was possible to neglect drop potentials and junction potentials on electrode/solution interfaces [10,34,42]. It is thus suitable to approximate $V_{rev}$ to $E_{diff}$. Finally, the complete analysis was carried out at pH = 10 because we have experimentally demonstrated that alkaline conditions increase the surface charge of PET channel and this fact triggered an enhancement of the performance (Figs. S4 and S5) [34,67]. Moreover, it has been recently reported that the increment of pH above 10 produces a reduction in the effective concentration gradient yielding a drop in the output power [68].

As anticipated in Fig. 3, the *i-V* curve measured under a concentration gradient is characterized by a non-zero potential ($V_{rev}$) at zero transmembrane current and a non-zero current ($i_0$) at zero transmembrane potential. The magnitude of these values is very sensitive to changes in the channel dimensions (Fig. 4A) [39]. A decrease in the effective channel diameter produces an increase in $V_{rev}$ and a decrease in $i_0$. Low inner space directly affects the ion flux which has a negative impact on $i_o$. On the other hand, the diminution of the effective channel size promotes the surface charge effect on the ionic transport which produces a more efficient exclusion of co-ions (nanoconfinement effect). This fact generates an enhancement in the junction potential that is translated into an increment of $V_{rev}$.

The dependence of the cation transference number on the effective size of the channels is shown in Fig. 4B. The transference number is commonly used as a measure of selectivity. For an ideal cation-selective system (carried out with KCl), $t_+$ tends towards 1 whereas for a non-selective system $t_+$ gets closer to 0.5. The cation-selectivity of the system increases with decreasing effective channel size due to the maximization of the relation between the EDL length and the channel size. In this condition, the increment of the electric potential perceived by the mobile ions yields an ion current with a predominant contribution of $K^+$. Fig. 4A and B show the dependence of $V_{rev}$, $i_o$, and $t_+$ as a function of the nanochannel effective diameters. These values were determined at a 1000-fold concentration gradient because this gradient condition presented the optimal results (Fig. S6).

To further analyze the ionic selectivity, the influence of gradient concentration on $t_+$ for the different channels was studied (Fig. 5). For this aim, the solution on the base side was 1 M KCl whereas the solution on the tip side was varied from $10^{-3}$ M to 0.1 M. The impact of the concentration gradient on the selectivity shows the same trend as the effective diameter. Increasing the ion concentration on the tip side of the nanochannel produces a drop in the EDL thickness and, therefore, in the electric surface potential perceived by the mobile ions. This fact leads to a decrease in the selectivity that is observed as a reduction of $t_+$, consistent with a diminution of log ($C_H/C_L$).

Output power (*P*) is a central parameter in blue energy devices and is obtained from the product of the current and the voltage. The maximum output power ($P_{max}$) is usually used as an indicator when evaluating the system performance. Taking into account that the power generation presents a maximum when V = $E_{diff}$/2, the maximum power transferable to an external source can be computed as follow [28],

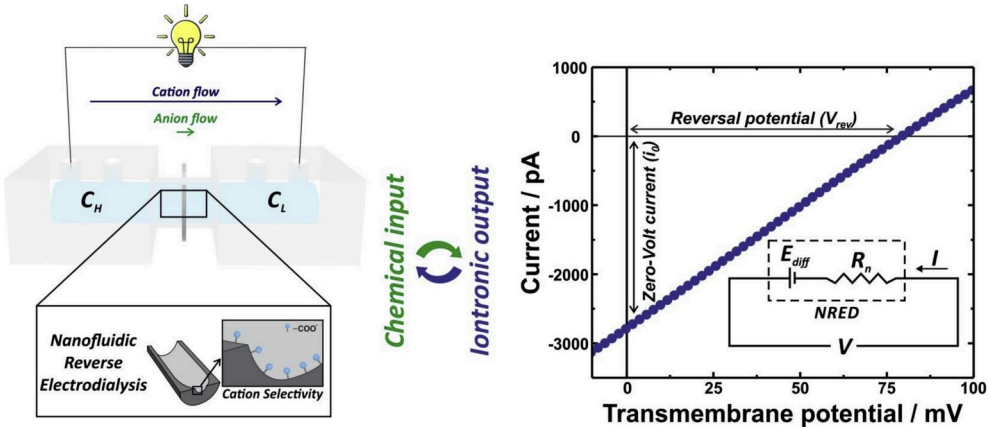


**Fig. 3. Left:** Scheme of the cell used for the *i-V* measurements. **Right**: *i-V* curve of a single nanochannel under to the application of a 100-fold KCl gradient. The chemical input, the iontronic output, and the equivalent circuit are also depicted.

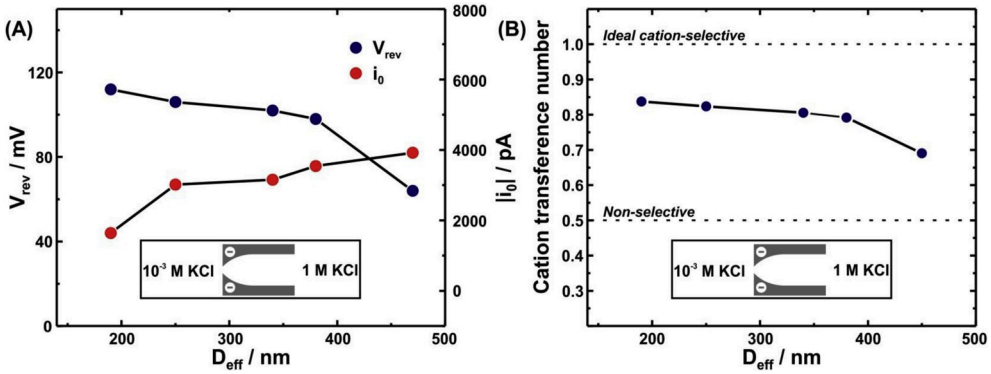


**Fig. 4.** (A) $i_o$ and $V_{rev}$ values obtained with bullet-shaped nanochannels with different values of $D_{eff}$. All measurements were carried out in a 1000-fold gradient at pH 10. (B) Cation transference number under a 1000-fold salinity gradient as a function of the effective diameter of the nanochannels.

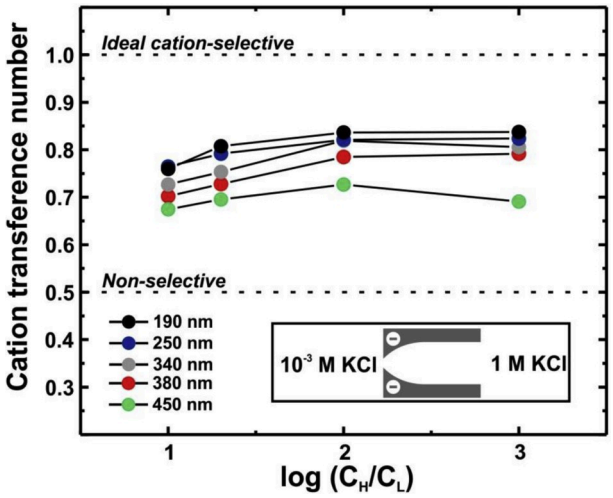


**Fig. 5.** Cation transference numbers for nanochannels of different diameters as a function of concentration gradient applied. The selectivity decreases for decreasing concentration gradients (increasing $C_L$). All measurements were carried out at pH = 10.

$$P_{\max} = \frac{E_{diff} i_o}{4} \tag{8}$$

In the following, we evaluate the performance of the nanochannel as an energy harvesting system based on the *i-V* curves. Fig. 6 shows the *i-V* and *Power-Voltage (P–V)* curves for different nanochannel sizes in the presence of a 1000-fold concentration gradient. In all cases, the *i-V* curves were linear in the exhibited transmembrane potential region (Fig. 6A). However, for larger potential windows, e. g. −1 to 1 V, the *i-V* curves showed a non-ohmic behavior (Fig. S7). Curves recorded under asymmetric electrolyte conditions presented a lower rectification efficiency than those recorded under symmetrical salt concentrations. The phenomenon is explained by the opposite direction of the ion diffusion generated by the gradient and the preferential direction of ion transport induced by the bullet-shaped geometry. This fact has been studied by other authors and is addressed in more detail in the **ESI** [69].

As shown in Fig. 4A, the increase in the effective pore diameter produces a diminution in $V_{rev}$ and an increment in the transmembrane current. This behavior has a direct impact on the *P–V* curves (Fig. 6B).

On the other hand, the nRED performance is very sensitive to the concentration gradient imposed (Fig. S6) [34]. In the gradient range employed, decreasing of $C_L$ produced both an increase in the $V_{rev}$ and $i_o$. For this reason, the maximum power estimated from eq. (8) increases as $C_H/C_L$ increases (Fig. 7A). Thus, enhancement in the maximum power output is possible via the maximization of the applied gradient. Fig. 7B presents the power and efficiency obtained for the different sizes applying a 1000-fold gradient. As it is shown in Fig. 4A, larger pore diameters produce higher $i_O$, but at the expense of a loss of selectivity (lower $V_{rev}$). This trend forced us to find the best condition at which the ionic flux could be maximized without appreciable loss of selectivity. The largest power generation is obtained for a channel of $D_{eff}$ = 380 nm with $P_{max}$ ~80 pW (Fig. 7B). This value widely exceeds the power generation values reported for similar bare PET channels without this bullet-shaped channel opening (Table 2). As an example, at pH = 7 with the application of 1000-fold gradient the $P_{max}$ values reported for cylindrical and conical PET channels do not exceed 10 pW [30,70], whereas for the present bullet-shaped nanochannel $P_{max}$ ~45 pW is obtained at the same experimental condition. Moreover, this value can be even maximized to 80 pW by increasing the pH to 10. These results

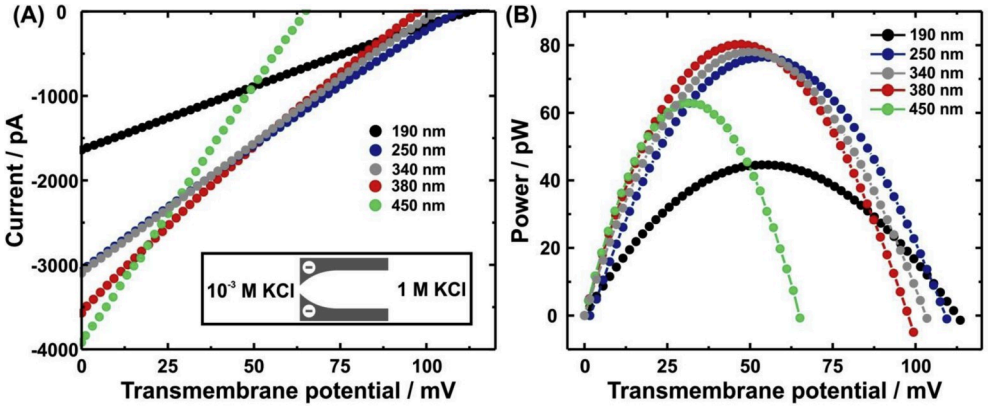


**Fig. 6.** (A) *i-V* curves and (B) P–V curves for the different channels with a gradient concentration of 1000-fold and pH = 10.

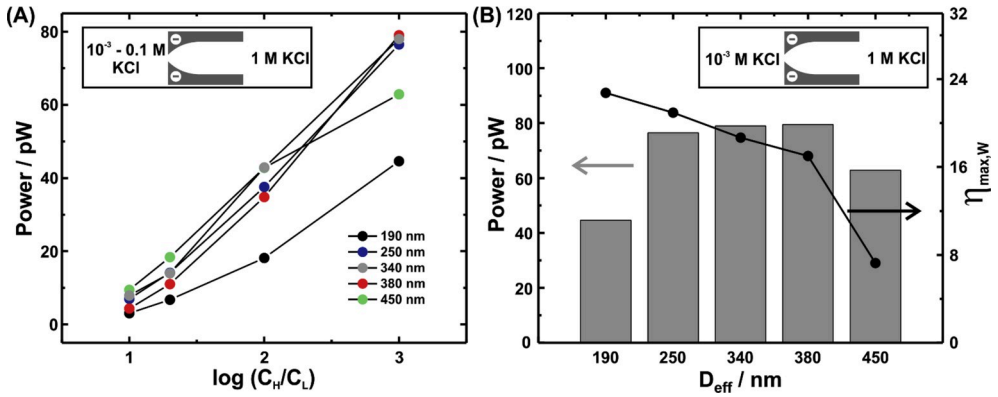


**Fig. 7.** (A) $P_{max}$ as a function of the concentration gradient for nanochannels of different diameters. (B) $P_{max}$ and energy conversion efficiency $\eta_{maxW}$ for different nanochannels applying an electrolyte gradient of 1000-fold. (x-axis not in scale). All measurements were carried out at pH = 10.

**Table 2**
Comparison between energy conversion devices based on PET membranes with different channel geometries and surface functionalization.

| Material | Description | $P_{max}$/ pW | Reference |
|---|---|---|---|
| PET | Conical channel modified with poly-Lysine | 120 | [31] |
| PET | Conical channel modified with chitosan and poly(acrylic acid) | 25 | [30] |
| PET | Conical bare channel (PET) | 5.2 | [30] |
| PET | Conical and cylindrical channel modified with cationic hydrogel | 20 | [70] |
| PET | Bare cylindrical channel | 0.2 | [76] |
| PET | Unmodified bullet-shaped channel | 80 | This work |

are in agreement with those obtained in previous works by PNP simulations, where better performance is obtained for bullet-shaped nanochannels in comparison with other geometries [38,40]. According to PNP simulations, the reason for higher power values would be the geometry of the bullet-shaped nanochannels, with larger channel volumes compared with other geometries [47,71]. Beyond the improvement in the selectivity obtained with conical-shaped nanochannels, the possibility of higher ionic current values can play a decisive role. For a bullet-shaped geometry, obviously the product of the current and the reversal potential becomes larger and thus beneficial for power generation. This fact is similar to the effect of geometry on the rectification efficiency where the larger currents exhibited in bullet-shaped channels are crucial too [47]. However, for the bullet-shaped nanochannels analyzed in this work no direct correlation is observed between the rectification efficiency and the maximum power obtained, suggesting a more complex relationship (Fig. S8). This is not surprising as for a given geometry, the maximum power generation as a function of the effective nanochannel diameters results from the compromise between two opposite effects: the increment of the ion-selective effects for lower diameters (yielding higher cation transfer numbers and $V_{rev}$ values) and the increment of the ionic current for higher diameters (yielding higher conductance and ionic currents). Of course, being the results of complex interplay, the optimum power becomes dependent on the experimental conditions. This compromise situation requires adjusting either the experimental conditions for a given nanochannel diameter or the effective size for a given operation condition to obtain the maximum power.

Finally, the enhanced performance of bullet-shaped nanochannels can be a key issue for the scaling-up to multi-pore membranes.

The energy conversion efficiency ($\eta$) is another important parameter in blue energy devices that accounts for the energy obtained compared to the energy entry. In mathematical terms, it is defined as the quotient between the electric energy generated and the energy entered to the system in terms of Gibbs free energy of mixing [72],

$$\eta = \frac{IV}{J_s RT \ln(a_H/a_L)} \tag{9}$$

where $J_s$ is the solute flux. For $P_{max}$ condition, the percentage of energy conversion efficiency is defined as $\eta_{maxW}$ estimated by the following equation [28],

$$\eta_{\max W} = \frac{(2t_+ - 1)^2}{2} 100 \tag{10}$$

The energy conversion efficiency f $\eta_{maxW}$ for the different effective channel diameters is shown in Fig. 7B. $\eta_{maxW}$ can be improved either by decreasing the nanochannel diameter or reducing the low concentration $C_L$ (Fig. S9).

The comparison with previous results obtained for single-channel membranes shows that experimentally the bullet-shaped geometry has a better performance than previous works with bare PET track-etched channels in terms of $P_{max}$ (Table 2). These results suggest that bullet-shaped nanochannels constitute promising candidates for the scaling to high-density pore membranes. It is important to mention that the scaling-up is not a trivial task and the linear estimation from single-channel to multi-channel systems leads to great uncertainties [36,73]. On the other hand, it also is important to remark that the present results were obtained with bare (unmodified) nanochannels. Even better performances either in terms of power or efficiency can be expected by appropriate surface functionalization methods [24,31,74,75].

By comparing with other nano/microfluidic systems, we can conclude that the nanofluidic system generated by ion-track-etching methods in polymer foils has great potential for the development of energy harvesting systems (Table 3). The power obtained exceeds several values reported previously for other materials. Based on the data presented here and in consonance with previous works, the ion-track-etching method constitutes a promising way for the development of high-power nRED systems that could provide a simple path for the design of low-cost power sources for microsystems.

## 4. Conclusions

The performance of PET membranes with a single bullet-shaped nanochannel was tested as an energy harvesting system under a variety of experimental conditions. The effect on performance was particularly investigated for various gradient concentrations and nanochannel diameters. In optimized conditions, a maximum output power of ~80 pW was obtained. This result widely exceeds the values reported previously for PET channels with conical and cylindrical geometries. The comparison in terms of maximum power for nRED systems based in inorganic materials demonstrates the high performance of tailored bullet-shaped track-etched channels. The flexibility of the ion-track

**Table 3**
Comparison of "blue energy" devices based on different materials and techniques.

| Material | Description | $P_{max}$/ pW | Reference |
|---|---|---|---|
| Polyimide | Track-etched Bare conical channel | 45 | [43] |
| Polyimide | Track-etched Bare conical channel | 26 | [34] |
| Silica | Silica nanochannels fabricated by glass-silicon anodic bonding | 0.16 | [28] |
| Silica | Silica nanochannel fabricated by electron beam lithography | 11 | [45] |
| Graphene | Single-layer graphene supported on PET foil | 41 | [77] |
| $MoS_2$ | $MoS_2$ nanochannel generated by electron irradiation under TEM or atomic scale ECR technique | ~18 | [78] |
| Boron nitride | *In-situ* SEM insertion of a nanotube in SiN membrane | 20 | [79] |
| PET | Unmodified bare bullet-shaped channel created by the ion-track-etching method | 80 | This work |

etching technique provides a great chance for the development of ion-selective membranes. The specific dependence of selectivity and power generation on channel size and shape as well as on the concentration gradient emphasizes the importance of carefully selecting adequate device design variables. Thus, the combination of channels with optimum geometrical parameters (shape, size, curvature, length, etc.) and appropriate experimental conditions (pH, concentration gradient, type of salt, etc.) is of paramount relevance facing to development of energy conversion systems with outstanding performance.

Besides the promising performance illustrated on bare nanochannels, it is important to note that the results can be further improved by means of surface modification techniques. The synergism between suitable modification and optimized geometry will be crucial for maximizing the performance of nRED systems.

## Declaration of competing interest

The authors declare that they have no known competing financial interests or personal relationships that could have appeared to influence the work reported in this paper.

## Acknowledgments

G.L. acknowledges a doctoral scholarship from CONICET. A.G.A., W. A.M. and O.A. are CONICET fellows and acknowledge financial support from Universidad Nacional de La Plata (PPID-X016), CONICET (PIP-0370) and ANPCyT (PICT-2017-1523 and PICT2016-1680). C.T. and M. E.T.M. acknowledge support by the LOEWE project iNAPO funded by the Hessen State Ministry of Higher Education, Research and Arts. The irradiated PET foils are part of the experiment UMAT, which was performed at the beam line X0 at the GSI Helmhotzzentrum fuer Schwerionenforschung, Darmstadt (Germany) in the frame of FAIR Phase-0. The authors acknowledge to Gonzalo Perez Mitta and Juan Allegretto for their fruitful discussions.

## Appendix A. Supplementary data

Supplementary data to this article can be found online at https://doi.org/10.1016/j.nanoen.2020.104612.

## References

[1] M.S. Dresselhaus, I.L. Thomas, Alternative energy technologies, Nature 414 (2001) 332.
[2] N.L. Panwar, S.C. Kaushik, S. Kothari, Role of renewable energy sources in environmental protection : a review, Renew. Sustain. Energy Rev. 15 (2011) 1513–1524, https://doi.org/10.1016/j.rser.2010.11.037.
[3] O. Ellabban, H. Abu-Rub, F. Blaabjerg, Renewable energy resources: current status, future prospects and their enabling technology, Renew. Sustain. Energy Rev. 39 (2014) 748–764, https://doi.org/10.1016/j.rser.2014.07.113.
[4] B.E. Logan, M. Elimelech, Membrane-based processes for sustainable power generation using water, Nature 488 (2012) 313–319, https://doi.org/10.1038/nature11477.
[5] G.Z. Ramon, B.J. Feinberg, E.M.V. Hoek, Membrane-based production of salinity-gradient power, Energy Environ. Sci. 4 (2011) 4423–4434, https://doi.org/10.1039/c1ee01913a.
[6] J.W. Post, J. Veerman, H.V.M. Hamelers, G.J.W. Euverink, S.J. Metz, K. Nymeijer, C.J.N. Buisman, Salinity-gradient power: evaluation of pressure-retarded osmosis and reverse electrodialysis, J. Membr. Sci. 288 (2007) 218–230, https://doi.org/10.1016/j.memsci.2006.11.018.
[7] J.W. Post, H.V.M. Hamelers, C.J.N. Buisman, Energy recovery from controlled mixing salt and fresh water with a reverse electrodialysis system, Environ. Sci. Technol. 42 (2008) 5785–5790, https://doi.org/10.1021/es8004317.
[8] Z. Jia, B. Wang, S. Song, Y. Fan, Blue energy : current technologies for sustainable power generation from water salinity gradient, Renew. Sustain. Energy Rev. 31 (2014) 91–100, https://doi.org/10.1016/j.rser.2013.11.049.
[9] N. Lakshminarayanaiah, Equations of Membrane Biophysics, Academic Press Inc., UK, 1984.
[10] A.J. Bard, L.R. Faulkner, Electrochemical Methods. Fundamentals and Applications, second ed., Wiley, USA, 2001.
[11] J. Cervera, A. Alcaraz, B. Schiedt, R. Neumann, P. Ramírez, Asymmetric selectivity of synthetic conical nanopores probed by reversal potential measurements, J. Phys. Chem. C 111 (2007) 12265–12273, https://doi.org/10.1021/jp071884c.
[12] Y. Mei, C.Y. Tang, Recent developments and future perspectives of reverse electrodialysis technology: a review, Desalination 425 (2018) 156–174, https://doi.org/10.1016/j.desal.2017.10.021.
[13] X. Chen, C. Li, M. Grätzel, R. Kostecki, S.S. Mao, Nanomaterials for renewable energy production and storage, Chem. Soc. Rev. 41 (2012) 7909, https://doi.org/10.1039/c2cs35230c.
[14] E. Serrano, G. Rus, J. García-Martínez, Nanotechnology for sustainable energy, Renew. Sustain. Energy Rev. 13 (2009) 2373–2384, https://doi.org/10.1016/j.rser.2009.06.003.
[15] J.G. Hong, H. Gao, L. Gan, X. Tong, C. Xiao, S. Liu, B. Zhang, Y. Chen, Nanocomposite and nanostructured ion-exchange membrane in salinity gradient power generation using reverse electrodialysis, in: Adv. Nanomater. Membr. Synth. Its Appl., Elsevier, 2019, pp. 295–316, https://doi.org/10.1016/B978-0-12-814503-6.00013-6.
[16] K. Kalyanasundaram, M. Grätzel, Themed issue : nanomaterials for energy conversion and storage, J. Mater. Chem. 22 (2012) 24190–24194, https://doi.org/10.1039/c2jm90163c.
[17] A. Siria, M. Bocquet, L. Bocquet, New avenues for the large-scale harvesting of blue energy, Nat. Rev. Chem. 1 (2016), 0091.
[18] N.S. Lewis, Toward cost-effective solar energy use, Science 315 (2007) 798–801, https://doi.org/10.1126/science.1137014.
[19] A.S. Aricò, P. Bruce, B. Scrosati, J.-M. Tarascon, W. van Schalkwijk, Nanostructured materials for advanced energy conversion and storage devices, Nat. Mater. 4 (2005) 366–377, https://doi.org/10.1038/nmat1368.
[20] G. Xie, L. Wen, L. Jiang, Biomimetic smart nanochannels for power harvesting, Nano Res. 9 (2016) 59–71, https://doi.org/10.1007/s12274-016-0993-1.
[21] L. Wen, Y. Tian, J. Ma, J. Zhai, L. Jiang, Construction of biomimetic smart nanochannels with polymer membranes and application in energy conversion systems, Phys. Chem. Chem. Phys. 14 (2012) 4027–4042, https://doi.org/10.1039/c2cp23911f.
[22] R. Li, X. Fan, Z. Liu, J. Zhai, Smart bioinspired nanochannels and their applications in energy-conversion systems, Adv. Mater. 29 (2017) 1702983, https://doi.org/10.1002/adma.201702983.
[23] K. Xiao, L. Jiang, M. Antonietti, Ion transport in nanofluidic devices for energy harvesting, Joule 3 (2019) 2364–2380, https://doi.org/10.1016/j.joule.2019.09.005.
[24] J. Gao, W. Guo, D. Feng, H. Wang, D. Zhao, L. Jiang, High-performance ionic diode membrane for salinity gradient power generation, J. Am. Chem. Soc. 136 (2014) 12265–12272, https://doi.org/10.1021/ja503692z.
[25] J. Kim, S.J. Kim, D.K. Kim, Energy harvesting from salinity gradient by reverse electrodialysis with anodic alumina nanopores, Energy 51 (2013) 413–421, https://doi.org/10.1016/j.energy.2013.01.019.
[26] R. Li, J. Jiang, Q. Liu, Z. Xie, J. Zhai, Hybrid nanochannel membrane based on polymer/MOF for high-performance salinity gradient power generation, Nano Energy 53 (2018) 643–649, https://doi.org/10.1016/j.nanoen.2018.09.015.
[27] S. Lee, H. Kim, D.-K. Kim, Power generation from concentration gradient by reverse electrodialysis in dense silica membranes for microfluidic and nanofluidic systems, Energies 9 (2016) 49, https://doi.org/10.3390/en9010049.
[28] D.K. Kim, C. Duan, Y.F. Chen, A. Majumdar, Power generation from concentration gradient by reverse electrodialysis in ion-selective nanochannels, Microfluid. Nanofluidics 9 (2010) 1215–1224, https://doi.org/10.1007/s10404-010-0641-0.
[29] Z. Zhang, X.Y. Kong, K. Xiao, Q. Liu, G. Xie, P. Li, J. Ma, Y. Tian, L. Wen, L. Jiang, Engineered asymmetric heterogeneous membrane: a concentration-gradient-driven energy harvesting device, J. Am. Chem. Soc. 137 (2015) 14765–14772, https://doi.org/10.1021/jacs.5b09918.
[30] S. Balme, T. Ma, E. Balanzat, J. Janot, Large osmotic energy harvesting from functionalized conical nanopore suitable for membrane applications, J. Membr. Sci. 544 (2017) 18–24, https://doi.org/10.1016/j.memsci.2017.09.008.
[31] C. Lin, C. Combs, Y. Su, L. Yeh, Z.S. Siwy, Rectification of concentration polarization in mesopores leads to high conductance ionic diodes and high

performance osmotic power, J. Am. Chem. Soc. 141 (2019) 3691–3698, https://doi.org/10.1021/jacs.8b13497.
[32] K. Kwon, S.J. Lee, L. Li, C. Han, D. Kim, Energy harvesting system using reverse electrodialysis with nanoporous polycarbonate track-etch membranes, Int. J. Energy Res. 38 (2014) 530–537, https://doi.org/10.1002/er.3111.
[33] J. Hwang, S. Kataoka, A. Endo, H. Daiguji, Enhanced energy harvesting by concentration gradient-driven ion transport in SBA-15 mesoporous silica thin films, Lab Chip 16 (2016) 3824–3832, https://doi.org/10.1039/c6lc00844e.
[34] W. Guo, L. Cao, J. Xia, F.Q. Nie, M. Wen, J. Xue, Y. Song, D. Zhu, Y. Wang, L. Jiang, Energy harvesting with single-ion-selective nanopores: a concentration-gradient-driven nanofluidic power source, Adv. Funct. Mater. 20 (2010) 1339–1344, https://doi.org/10.1002/adfm.200902312.
[35] Z. Siwy, I.D. Kosińska, A. Fuliński, C.R. Martin, Asymmetric diffusion through synthetic nanopores, Phys. Rev. Lett. 94 (2005) 1–4, https://doi.org/10.1103/PhysRevLett.94.048102.
[36] J. Su, D. Ji, J. Tang, H. Li, Y. Feng, L. Cao, L. Jiang, W. Guo, Anomalous pore-density dependence in nanofluidic osmotic power generation, Chin. J. Chem. 36 (2018) 417–420, https://doi.org/10.1002/cjoc.201800067.
[37] J. Gao, X. Liu, Y. Jiang, L. Ding, L. Jiang, W. Guo, Understanding the giant gap between single-pore- and membrane-based nanofluidic osmotic power generators, Small 1804279 (2019) 1–8, https://doi.org/10.1002/smll.201804279.
[38] J.-P. Hsu, T.-C. Su, C.-Y. Lin, S. Tseng, Power generation from a pH-regulated nanochannel through reverse electrodialysis: effects of nanochannel shape and non-uniform H+ distribution, Electrochim. Acta 294 (2019) 84–92, https://doi.org/10.1016/j.electacta.2018.10.074.
[39] S. Tseng, Y.M. Li, C.Y. Lin, J.P. Hsu, Salinity gradient power: influences of temperature and nanopore size, Nanoscale 8 (2016) 2350–2357, https://doi.org/10.1039/c5nr07563g.
[40] J. Cervera, P. Ramirez, S. Mafe, P. Stroeve, Asymmetric nanopore rectification for ion pumping, electrical power generation, and information processing applications, Electrochim. Acta 56 (2011) 4504–4511, https://doi.org/10.1016/j.electacta.2011.02.056.
[41] S. Tseng, Y. Li, C. Lin, J. Hsu, Salinity gradient power : optimization of nanopore size, Electrochim. Acta 219 (2016) 790–797, https://doi.org/10.1016/j.electacta.2016.10.014.
[42] P. Ramirez, J. Cervera, V. Gomez, M. Ali, S. Nasir, W. Ensinger, S. Mafe, Membrane potential of single asymmetric nanopores : divalent cations and salt mixtures, J. Membr. Sci. 573 (2019) 579–587, https://doi.org/10.1016/j.memsci.2018.12.043.
[43] L. Cao, W. Guo, W. Ma, L. Wang, F. Xia, S. Wang, Y. Wang, L. Jiang, D. Zhu, Towards understanding the nanofluidic reverse electrodialysis system: well matched charge selectivity and ionic composition, Energy Environ. Sci. 4 (2011) 2259–2266, https://doi.org/10.1039/c1ee01088c.
[44] L. Cao, F. Xiao, Y. Feng, W. Zhu, W. Geng, J. Yang, X. Zhang, N. Li, W. Guo, L. Jiang, Anomalous channel-length dependence in nanofluidic osmotic energy conversion, Adv. Funct. Mater. 27 (2017) 1604302, https://doi.org/10.1002/adfm.201604302.
[45] Y. Zhang, Z. Huang, Y. He, X. Miao, Enhancing the efficiency of energy harvesting from salt gradient with ion-selective nanochannel, Nanotechnology 146 (2019) 428–429, https://doi.org/10.1088/1361-6528/ab0ed8.
[46] Y. He, Z. Huang, B. Chen, M. Tsutsui, X. Shui Miao, M. Taniguchi, Electrokinetic analysis of energy harvest from natural salt gradients in nanochannels, Sci. Rep. 7 (2017) 13156, https://doi.org/10.1038/s41598-017-13336-w.
[47] P. Ramírez, P.Y. Apel, J. Cervera, S. Mafé, Pore structure and function of synthetic nanopores with fixed charges: tip shape and rectification properties, Nanotechnology 19 (2008) 315707, https://doi.org/10.1088/0957-4484/19/31/315707.
[48] P.Y. Apel, I.V. Blonskaya, S.N. Dmitriev, O.L. Orelovitch, A. Presz, B.A. Sartowska, Fabrication of nanopores in polymer foils with surfactant-controlled longitudinal profiles, Nanotechnology 18 (2007) 305302, https://doi.org/10.1088/0957-4484/18/30/305302.
[49] R. Spohr, Ion Tracks and Microtechnology: Principles and Applications, first ed., Vieweg+Teubner Verlag, 1990.
[50] P.Y. Apel, I.V. Blonskaya, A.Y. Didyk, S.N. Dmitriev, O.L. Orelovitch, D. Root, L. I. Samoilova, V.A. Vutsadakis, Surfactant-enhanced control of track-etch pore morphology, Nucl. Instrum. Methods Phys. Res. Sect. B Beam Interact. Mater. Atoms 179 (2001) 55–62, https://doi.org/10.1016/S0168-583X(00)00691-1.
[51] P.Y. Apel, V.V. Bashevoy, I.V. Blonskaya, N.E. Lizunov, O.L. Orelovitch, C. Trautmann, Shedding light on the mechanism of asymmetric track etching: an interplay between latent track structure, etchant diffusion and osmotic flow, Phys. Chem. Chem. Phys. 18 (2016) 25421–25433, https://doi.org/10.1039/C6CP05465J.
[52] G. Laucirica, G. Pérez-Mitta, M.E. Toimil-Molares, C. Trautmann, W.A. Marmisollé, O. Azzaroni, Amine-phosphate specific interactions within nanochannels: binding behavior and nanoconfinement effects, J. Phys. Chem. C (2019), https://doi.org/10.1021/acs.jpcc.9b07977.
[53] Gamry Instruments, Two, Three and Four Electrode Experiments, 2013. https://www.gamry.com/application-notes/electrodes-cells/two-three-and-four-electrode-experiments/.
[54] A. Wolf, N. Reber, P.Y. Apel, B.E. Fischer, R. Spohr, Electrolyte transport in charged single ion track capillaries, Nucl. Instrum. Methods Phys. Res. B. 105 (1995) 291–293.
[55] J.F. Pietschmann, M.T. Wolfram, M. Burger, C. Trautmann, G. Nguyen, M. Pevarnik, V. Bayer, Z. Siwy, Rectification properties of conically shaped nanopores: consequences of miniaturization, Phys. Chem. Chem. Phys. 15 (2013) 16917–16926, https://doi.org/10.1039/c3cp53105h.
[56] Z.S. Siwy, Ion-current rectification in nanopores and nanotubes with broken symmetry, Adv. Funct. Mater. 16 (2006) 735–746, https://doi.org/10.1002/adfm.200500471.
[57] R.B. Schoch, J. Han, P. Renaud, Transport phenomena in nanofluidics, Rev. Mod. Phys. 80 (2008) 839–883, https://doi.org/10.1103/RevModPhys.80.839.
[58] J. Cervera, B. Schiedt, R. Neumann, S. Mafé, P. Ramírez, Ionic conduction, rectification, and selectivity in single conical nanopores, J. Chem. Phys. 124 (2006) 104706, https://doi.org/10.1063/1.2179797.
[59] H. Daiguji, Ion transport in nanofluidic channels, Chem. Soc. Rev. 39 (2010) 901–911, https://doi.org/10.1039/B820556F.
[60] P.Y. Apel, I.V. Blonskaya, N.V. Levkovich, O.L. Orelovich, Asymmetric track membranes: relationship between nanopore geometry and ionic conductivity, Petrol. Chem. 51 (2011) 555–567, https://doi.org/10.1134/S0965544111070024.
[61] P.Y. Apel, I.V. Blonskaya, N.E. Lizunov, K. Olejniczak, O.L. Orelovitch, B. A. Sartowska, S.N. Dmitriev, Asymmetrical nanopores in track membranes: fabrication, the effect of nanopore shape and electric charge of pore walls, promising applications, Russ. J. Electrochem. 53 (2017) 58–69, https://doi.org/10.1134/s1023193517010037.
[62] R.B. Schoch, P. Renaud, Ion transport through nanoslits dominated by the effective surface charge, Appl. Phys. Lett. 86 (2005) 1–3, https://doi.org/10.1063/1.1954899.
[63] J. Wang, M. Zhang, J. Zhai, L. Jiang, Theoretical simulation of the ion current rectification (ICR) in nano-pores based on the Poisson-Nernst-Planck (PNP) model, Phys. Chem. Chem. Phys. 16 (2014) 23–32, https://doi.org/10.1039/c3cp51712h.
[64] P.Y. Apel, I.V. Blonskaya, O.L. Orelovitch, P. Ramirez, B.A. Sartowska, Effect of nanopore geometry on ion current rectification, Nanotechnology 22 (2011) 175302, https://doi.org/10.1088/0957-4484/22/17/175302.
[65] H.C. Yeh, C.C. Chang, R.J. Yang, Reverse electrodialysis in conical-shaped nanopores: salinity gradient-driven power generation, RSC Adv. 4 (2014) 2705–2714, https://doi.org/10.1039/c3ra45392h.
[66] W.J. Hamer, Y. Wu, Osmotic coefficients and mean activity coefficients of uni-univalent electrolytes in water at 25°C, J. Phys. Chem. Ref. Data 1 (1972) 1047–1100, https://doi.org/10.1063/1.3253108.
[67] J.P. Hsu, T.C. Su, C.Y. Lin, S. Tseng, Power generation from a pH-regulated nanochannel through reverse electrodialysis: effects of nanochannel shape and non-uniform H+ distribution, Electrochim. Acta 294 (2019) 84–92, https://doi.org/10.1016/j.electacta.2018.10.074.
[68] J.-P. Hsu, T.-C. Su, P.-H. Peng, S.-C. Hsu, M.-J. Zheng, L.-H. Yeh, Unraveling the anomalous surface-charge-dependent osmotic power using a single funnel-shaped nanochannel, ACS Nano (2019), https://doi.org/10.1021/acsnano.9b06774.
[69] L. Cao, W. Guo, Y. Wang, L. Jiang, Concentration-gradient-dependent ion current rectification in charged conical nanopores, Langmuir 28 (2012) 2194–2199, https://doi.org/10.1021/la203837q.
[70] T. Ma, E. Balanzat, J.-M. Janot, S. Balme, Nanopore functionalized by highly charged hydrogels for osmotic energy harvesting, ACS Appl. Mater. Interfaces 11 (2019) 12578–12585, https://doi.org/10.1021/acsami.9b01768.
[71] J. Cervera, P. Ramirez, S. Mafe, P. Stroeve, Asymmetric nanopore rectification for ion pumping, electrical power generation, and information processing applications, Electrochim. Acta 56 (2011) 4504–4511, https://doi.org/10.1016/j.electacta.2011.02.056.
[72] J.C. Fair, J.F. Osterle, Reverse electrodialysis in charged capillary membranes, J. Chem. Phys. 54 (1971) 3307, https://doi.org/10.1063/1.1675344.
[73] F. Xiao, D. Ji, H. Li, J. Tang, Y. Feng, L. Ding, L. Cao, N. Li, L. Jiang, W. Guo, A general strategy to simulate osmotic energy conversion in multi-pore nanofluidic systems, Mater. Chem. Front. 2 (2018) 935–941, https://doi.org/10.1039/C8QM00031J.
[74] J. Zhang, N. Liu, B. Wei, X. Ou, X. Xu, X. Lou, F. Xia, The opposite gating behaviors of solid-state nanochannels modified with long and short polymer chains, Chem. Commun. 51 (2015) 10146–10149, https://doi.org/10.1039/c5cc02774h.
[75] M. Macha, S. Marion, V.V.R. Nandigana, A. Radenovic, 2D materials as an emerging platform for nanopore-based power generation, Nat. Rev. Mater. 4 (2019) 588–605, https://doi.org/10.1038/s41578-019-0126-z.
[76] Y. Xie, X. Wang, J. Xue, K. Jin, L. Chen, Y. Wang, Electric energy generation in single track-etched nanopores, Appl. Phys. Lett. 93 (2008) 163116, https://doi.org/10.1063/1.3001590.
[77] Y. Fu, X. Guo, Y. Wang, X. Wang, J. Xue, An atomically-thin graphene reverse electrodialysis system for efficient energy harvesting from salinity gradient, Nano Energy 57 (2019) 783–790, https://doi.org/10.1016/j.nanoen.2018.12.075.
[78] J. Feng, M. Graf, K. Liu, D. Ovchinnikov, D. Dumcenco, M. Heiranian, V. Nandigana, N.R. Aluru, A. Kis, A. Radenovic, Single-layer MoS2nanopores as nanopower generators, Nature 536 (2016) 197–200, https://doi.org/10.1038/nature18593.
[79] A. Siria, P. Poncharal, A. Biance, R. Fulcrand, X. Blasé, S.T. Purcell, L. Bocquet, Giant osmotic energy conversion measured in a single transmembrane boron nitride nanotube, Nature 494 (2013) 455–458, https://doi.org/10.1038/nature11876.